





Cluster analysis to identify long COVID phenotypes using ^{129}Xe magnetic resonance imaging: a multicentre evaluation

Rachel L. Eddy ^{1,2}, David Mummy³, Shuo Zhang³, Haoran Dai⁴, Aryil Bechtel³, Alexandra Schmidt¹, Bradie Frizzell⁵, Firoozeh V. Gerayeli¹, Jonathon A. Leipsic^{1,6}, Janice M. Leung^{1,2}, Bastiaan Driehuys^{3,4,7}, Loretta G. Que ⁸, Mario Castro⁵, Don D. Sin^{1,2} and Peter J. Niedbalski⁵

¹Centre for Heart Lung Innovation, St Paul's Hospital, University of British Columbia, Vancouver, BC, Canada. ²Division of Respiratory Medicine, Department of Medicine, University of British Columbia, Vancouver, BC, Canada. ³Department of Radiology, Duke University, Durham, NC, USA. ⁴Department of Medical Physics, Duke University, Durham, NC, USA. ⁵Division of Pulmonary and Critical Care Medicine, University of Kansas Medical Center, Kansas City, KS, USA. ⁶Department of Radiology, University of British Columbia, Vancouver, BC, Canada. ⁷Department of Biomedical Engineering, Duke University, Durham, NC, USA. ⁸Division of Pulmonary, Department of Medicine, Duke University, Durham, NC, USA.

Corresponding author: Peter J. Niedbalski (pniedbalski@kumc.edu)



Shareable abstract (@ERSpublications)

Cluster analysis of ^{129}Xe MRI metrics identifies 4 phenotypes of long COVID with distinct functional MRI and clinical characteristics. MRI-based clusters can be used to dissect long COVID heterogeneity, enabling personalised clinical care and treatment. <https://bit.ly/42uia1J>

Cite this article as: Eddy RL, Mummy D, Zhang S, *et al.* Cluster analysis to identify long COVID phenotypes using ^{129}Xe magnetic resonance imaging: a multicentre evaluation. *Eur Respir J* 2024; 63: 2302301 [DOI: 10.1183/13993003.02301-2023].

Copyright ©The authors 2024.

This version is distributed under the terms of the Creative Commons Attribution Non-Commercial Licence 4.0. For commercial reproduction rights and permissions contact permissions@ersnet.org

This article has an editorial commentary: <https://doi.org/10.1183/13993003.00381-2024>

Received: 26 Oct 2023
Accepted: 26 Jan 2024

Abstract

Background Long COVID impacts ~10% of people diagnosed with coronavirus disease 2019 (COVID-19), yet the pathophysiology driving ongoing symptoms is poorly understood. We hypothesised that ^{129}Xe magnetic resonance imaging (MRI) could identify unique pulmonary phenotypic subgroups of long COVID. Therefore, we evaluated ventilation and gas exchange measurements with cluster analysis to generate imaging-based phenotypes.

Methods COVID-negative controls and participants who previously tested positive for COVID-19 underwent ^{129}Xe MRI ~14 months post-acute infection across three centres. Long COVID was defined as persistent dyspnoea, chest tightness, cough, fatigue, nausea and/or loss of taste/smell at MRI; participants reporting no symptoms were considered fully recovered. ^{129}Xe MRI ventilation defect percent (VDP) and membrane-to-gas (Mem/Gas), red blood cell-to-membrane (RBC/Mem) and red blood cell-to-gas (RBC/Gas) ratios were used in k-means clustering for long COVID, and measurements were compared using ANOVA with post-hoc Bonferroni correction.

Results We evaluated 135 participants across three centres: 28 COVID-negative (mean±SD age 40±16 years), 34 fully recovered (42±14 years) and 73 long COVID (49±13 years). RBC/Mem ($p=0.03$) and forced expiratory volume in 1 s (FEV_1) ($p=0.04$) were different between long COVID and COVID-negative; FEV_1 and all other pulmonary function tests (PFTs) were within normal ranges. Four unique long COVID clusters were identified compared with recovered and COVID-negative. Cluster 1 was the youngest with normal MRI and mild gas trapping; Cluster 2 was the oldest, characterised by reduced RBC/Mem but normal PFTs; Cluster 3 had mildly increased Mem/Gas with normal PFTs; and Cluster 4 had markedly increased Mem/Gas with concomitant reduction in RBC/Mem and restrictive PFT pattern.

Conclusions We identified four ^{129}Xe MRI long COVID phenotypes with distinct characteristics. ^{129}Xe MRI can dissect pathophysiological heterogeneity of long COVID to enable personalised patient care.

Introduction

As the world transitions to a post-pandemic stage of coronavirus disease 2019 (COVID-19), clinical and research focus has shifted from the acute to chronic effects. Long COVID (also known as post-COVID syndrome or post-acute sequelae of COVID) is broadly accepted as signs, symptoms and/or conditions that continue or develop >4–12 weeks following acute infection [1–3]. Long COVID has been estimated to



affect ~10% of the over 770 million individuals who experienced severe acute respiratory syndrome coronavirus 2 (SARS-CoV-2) infection [4–7] and may persist for ≥ 2 years [8]. While it is now clear that long COVID is a multi-organ condition with a wide range of symptoms frequently involving the respiratory system [6, 9], pulmonary function tests (PFTs) and conventional computed tomography (CT) are typically normal. Since the physiological drivers of persistent symptoms in these people are not fully understood, it remains difficult to manage the varied symptoms of long COVID patients and to identify effective therapies.

One important challenge in identifying novel therapies in long COVID is its heterogeneity. Imaging has the potential to reveal unique phenotypes of long COVID. Functional evaluation using expiratory CT and hyperpolarised ^{129}Xe magnetic resonance imaging (MRI) have revealed air trapping [10] and ventilation abnormalities [11, 12] in people reporting long COVID, suggesting the importance of small airway dysfunction in the pathophysiology. ^{129}Xe MRI further enables measurement of regional gas exchange as inhaled ^{129}Xe gas uptake in the alveolar membrane and transfer to capillary red blood cells, and in long COVID has characteristically shown reduced ^{129}Xe red blood cell-to-membrane (RBC/Mem) ratio [13–17]. These findings have been postulated to reflect microvascular abnormalities [13, 16, 18] and have been observed in people with dyspnoea [13–15] or any other persistent symptoms [16, 17], those who have been hospitalised [13–17] or not [16, 17], for ≥ 1 year after acute infection [15, 17], and importantly when conventional CT and PFTs have been mostly normal.

Given the broad range of long COVID presentation, there have been efforts to define phenotypes or clusters using symptoms or clinical factors [19–21]. Such phenotypic clustering has also been pursued in asthma and COPD using CT and ^{129}Xe MRI metrics to identify distinct lung structure–function and clinical characteristics that were not distinguishable using clinical evaluations alone [22–24]. We therefore hypothesised that ^{129}Xe MRI could also identify unique pulmonary phenotypic subgroups of long COVID. Thus, in this study we evaluated MRI gas exchange and ventilation measurements in participants with long COVID across three centres, and employed a cluster analysis to generate imaging-based phenotypes of long COVID and to determine the relation of these phenotypes to clinical end-points such as symptoms. Preliminary results have been reported in abstract form [25].

Materials and methods

Study participants and design

Participants aged ≥ 19 years who self-reported a previous positive test for COVID-19 by a PCR or lateral flow test provided written informed consent to ethics board-approved protocols between July 2021 and February 2023 across three academic centres: University of British Columbia (Vancouver, BC, Canada; Site 1), University of Kansas Medical Center (Kansas City, KS, USA; Site 2) and Duke University (Durham, NC, USA; Site 3). At all centres participants were recruited through referral from healthcare providers or community advertising and study assessments were completed ≥ 3 months after the COVID-19 test date. Participants were not recruited by any specific symptoms and participants reporting no symptoms (*i.e.* no long COVID) were also recruited (Site 1 and Site 2). Participants with pre-existing respiratory disease were not excluded. COVID-negative healthy controls were prospectively recruited (Site 1) or retrospectively included from pre-existing datasets (Site 2 and Site 3).

All participants underwent hyperpolarised ^{129}Xe gas exchange MRI, while PFT measurements and chest CT performed in the respective clinical laboratories/departments were included where available. Board-certified radiologist reports for inspiratory CT performed within 6 months of MRI were reviewed for the presence of ground-glass opacities (GGOs), reticulation, honeycombing, consolidation and emphysema. The following self-reported (new or worsened) persistent symptoms for >3 months post-COVID (yes/no) were recorded across all sites at the time of MRI: dyspnoea, chest tightness, cough, fatigue, nausea and loss of taste/smell. Long COVID was defined when at least one of these symptoms was present, new/worse post-COVID, and not explained by another cause as adjudicated by site investigators. Participants reporting no symptoms were considered fully recovered. The St George's Respiratory Questionnaire (SGRQ) was also administered at Site 1 to measure respiratory-related quality of life [26].

Pulmonary function tests

Spirometry was performed according to American Thoracic Society/European Respiratory Society guidelines [27] to determine forced expiratory volume in 1 s (FEV_1) and forced vital capacity (FVC), and plethysmography [28] was performed to measure residual volume (RV) and total lung capacity (TLC). Diffusion capacity of the lung for carbon monoxide (D_{LCO}) was measured using the single-breath method [29]. All values were reported using race-neutral Global Lung Function Initiative reference equations [30].

MRI acquisition and analysis

MRI was performed using 3T MAGNETOM systems (Site 1: Vida; Site 2: Skyra; Site 3: PrismaFIT; Siemens Healthineers, Erlangen, Germany) and a flexible ^{129}Xe vest coil (Clinical MR Solutions, Brookfield, WI, USA). Up to 1.0 L of isotopically enriched ($\geq 85\%$) ^{129}Xe gas was polarised using 9820 hyperpolarisers (Polarean Imaging, Durham, NC, USA). Total inhaled doses were 1.0 L (Site 1) or 20% of the participants' FVC up to a maximum of 1.25 L (Site 2 and Site 3) and participants were instructed to inhale the gas mixture from functional residual capacity for imaging under breath-hold conditions. Gas exchange imaging was performed using single-breath 1-point Dixon methods (Site 1 [31], Site 2 [32] and Site 3 [33]) to generate simultaneous ^{129}Xe gas and dissolved phase images (xenon dissolved in interstitial membrane and red blood cells within the pulmonary capillaries). Minor variations in flip angle, repetition time (TR) and sampling strategy were used in the 1-point Dixon methods across sites. The modified methods primarily reduced acquisition time [32, 33] and have been validated against the gold standard [31] to maintain quantitative gas exchange measurements. Importantly, the equivalent TR for a hypothetical 90° flip angle ($\text{TR}_{90,\text{equiv}}$), which determines gas exchange image contrast, was 249 ms across all sites, enabling meaningful aggregation of the multicentre data. Detailed MRI protocols are described in the supplementary material.

Quantitative MRI analysis was performed centrally at Site 3 as previously described [34]. Ventilation defect percent (VDP) was quantified as the percentage of lung with absent ^{129}Xe gas signal, reflecting airway obstruction and flow limitation. Gas exchange was quantified as whole-lung membrane-to-gas (Mem/Gas), RBC/Mem and red blood cell-to-gas (RBC/Gas) ratios. Mem/Gas, or membrane tissue uptake, measures ^{129}Xe dissolved in the interstitial membrane normalised to the gas signal and reflects parenchymal integrity; high membrane uptake is typically due to fibrosis or inflammation whereas low membrane uptake is typically due to tissue destruction or emphysema. RBC/Gas, or red blood cell transfer, measures ^{129}Xe dissolved in pulmonary capillary red blood cells normalised to the gas signal and reflects microvascular integrity; low RBC/Gas is typically due to diffusion/perfusion limitation or vascular destruction. RBC/Mem measures the ratio of ^{129}Xe dissolved in red blood cells to that in interstitial tissue and represents the efficiency of transfer of gas from the interstitium to capillary red blood cells as a measure of overall gas exchange; reduced RBC/Mem could be due to reduced red blood cell transfer and/or increased membrane uptake. RBC/Mem has been most widely applied to date to evaluate long COVID [13–17]. MRI measurements were not adjusted for haemoglobin, consistent with prior work in this area. VDP, Mem/Gas, RBC/Mem and RBC/Gas were included for clustering to represent the range of pulmonary pathophysiology including airway, parenchymal and microvascular measurements from a single ^{129}Xe scan.

Statistical analysis

Clustering was performed for long COVID participants using MATLAB R2021a (MathWorks, Natick, MA, USA). MRI variables were z-transformed to standardise scales and k-means clustering was performed for two to five clusters. Internal cluster validation to determine the optimal number of clusters was evaluated using the following parameters: Davies–Bouldin index, measuring the average similarity between clusters (minimised); silhouette width, measuring the average distance between clusters (maximised); and Dunn's index, measuring the ratio of smallest distance between observations in different clusters to the largest cluster diameter (maximised).

All statistical analysis was performed using SPSS Statistics version 25.0 (IBM, Armonk, NY, USA). Data were tested for normality using Shapiro–Wilk tests and when not normally distributed, non-parametric tests were performed. Numerical variables were compared using ANOVA or Kruskal–Wallis tests with a post-hoc Bonferroni correction for multiple comparisons unless otherwise stated. Categorical variables were compared using Fisher's exact test. Relationships were evaluated using Spearman correlation coefficients. Results were considered statistically significant when $p < 0.05$.

Results

Figure 1 shows the flow diagram of participant enrolment from each site; in total, we evaluated 135 participants across three centres, including 28 COVID-negative participants (mean \pm SD age 40 \pm 16 years; 16 females), 34 fully recovered from COVID-19 (42 \pm 14 years; 19 females) and 73 with long COVID (49 \pm 13 years; 43 females). Table 1 shows participant demographics, lung function and imaging measurements by group. All groups were predominantly White Caucasians (>75%); 12% of the fully recovered and 25% of long COVID participants were hospitalised during the acute infection. Time between COVID-19 diagnosis and MRI was not significantly different between the fully recovered and long COVID participants (mean \pm SD 424 \pm 243 versus 414 \pm 226 days; median (interquartile range) 399 (223–610) versus 405 (217–565) days; both $p = 0.8$). Long COVID participants were significantly older than COVID-negative ($p = 0.01$) with significantly higher SGRQ scores ($p < 0.001$ versus COVID-negative and recovered) and significantly lower ^{129}Xe RBC/Mem ($p = 0.03$). FEV_1 was also significantly lower in long

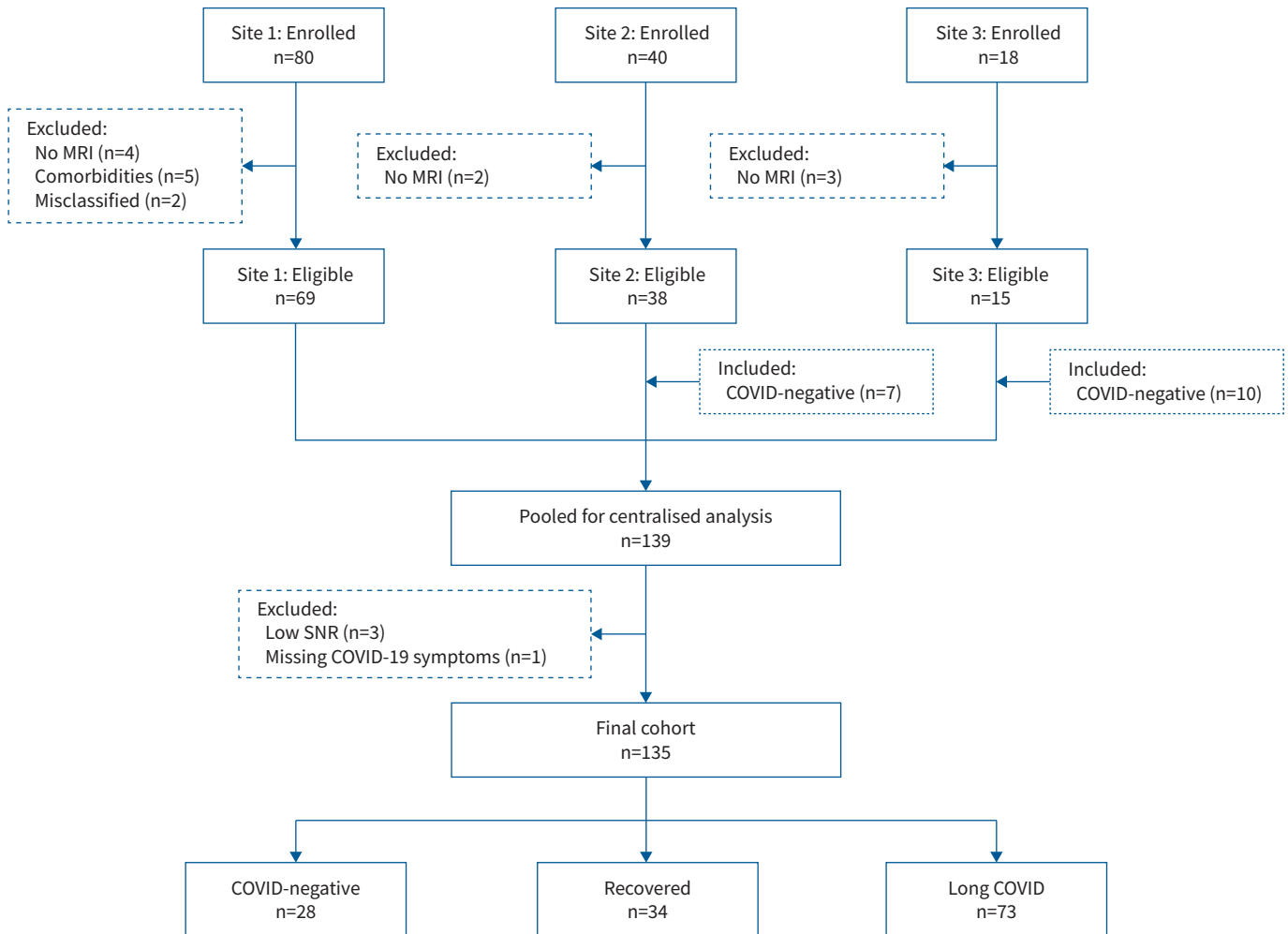


FIGURE 1 CONSORT (Consolidated Standards of Reporting Trials) flow diagram of enrolment of participants. Of 80 participants enrolled at Site 1, nine were excluded (four did not complete magnetic resonance imaging (MRI) and five were COVID-negative or fully recovered with comorbidities or exposures that could influence ^{129}Xe MRI (severe COPD (n=2), rheumatoid arthritis (n=1), HIV (n=1), and heavy current daily cannabis and tobacco smoking (n=1))) and two were deemed misclassified (no positive coronavirus disease 2019 (COVID-19) test and negative antibody test (n=1), and positive COVID-19 test between pulmonary function tests and MRI (n=1)). Site 2 and Site 3 enrolled 40 and 18 participants, respectively, of which two at Site 2 and three at Site 3 did not complete MRI and were excluded. Site 2 (n=7) and Site 3 (n=10) retrospectively included COVID-negative controls, whereas Site 1 prospectively enrolled. From 139 participants pooled for centralised analysis, four were further excluded (low ^{129}Xe gas signal-to-noise ratio (SNR) (n=3) and missing COVID-19 symptoms for classification as recovered or long COVID (n=1)) and the final study group consisted of 135 participants in total (n=28 COVID-negative, n=34 fully recovered and n=73 long COVID).

COVID ($p=0.04$) but was within normal limits; all other PFT measurements were also within normal limits and not significantly different. ^{129}Xe VDP, Mem/Gas, RBC/Mem and RBC/Gas plotted by group are shown in supplementary figure E1. Supplementary tables E1–E3 show study measurements by site for each group.

Figure 2a shows that the optimal number of clusters was four, all of which contained participants from each site (supplementary table E4). Figure 2b shows a radar plot of the primary MRI signatures associated with each of the four clusters. Qualitatively, VDP did not largely contribute to any group but was greatest in Cluster 2. Mem/Gas was greatest in Cluster 3 and Cluster 4, and RBC/Mem and RBC/Gas were lowest in Cluster 2 and Cluster 4.

Table 2 provides a full listing of measurements, self-reported pre-existing comorbidities and persistent symptoms, and CT patterns by cluster. The time between COVID-19 diagnosis and MRI was not significantly different across the clusters nor was the proportion of participants by sex or SGRQ Total, Symptom and Impact scores ($p>0.1$). SGRQ Activity score was significantly different ($p=0.02$), with the

TABLE 1 Participant demographic, pulmonary function test (PFT)[#] and magnetic resonance imaging (MRI) measurements

	COVID-negative (n=28)	Recovered (n=34)	Long COVID (n=73)	p-value [¶]
Age (years)	40±16	42±14	49±12 [§]	0.004
Female	16 (57)	20 (59)	44 (60)	1.0
Caucasian	22 (79)	28 (82)	62 (85)	0.3
BMI (kg·m ⁻²)	27±4	27±5	29±6	0.2
Hospitalised for COVID-19 during acute infection		4 (12)	18 (25)	0.2
Time between COVID-19 diagnosis and MRI (days)		424±243	414±226	0.8
SGRQ Total [†]	5±5	7±7	36±20 ^{§,f}	<0.001
SGRQ Symptom [†]	5±7	11±14	42±22 ^{§,f}	<0.001
SGRQ Activity [†]	10±12	12±11	51±26 ^{§,f}	<0.001
SGRQ Impact [†]	1±3	3±6	26±21 ^{§,f}	<0.001
FEV ₁ (% pred)	105±15	109±16	99±18 ^f	0.04
FVC (% pred)	107±13	112±15	102±20	0.06
FEV ₁ /FVC (%)	81±8	80±7	79±6	0.5
RV (% pred)	108±25	110±21	106±30	0.8
TLC (% pred)	99±13	102±11	94±18	0.09
RV/TLC (% pred)	107±19	109±19	112±22	0.6
D _{LCO} (% pred)	103±14	108±10	99±24	0.1
VDP (%)	0±1	0±1	1±2	0.2
Mem/Gas (×10 ⁻²)	0.71±0.15	0.73±0.18	0.77±0.24	0.4
RBC/Mem	0.47±0.13	0.43±0.11	0.40±0.12 [§]	0.03
RBC/Gas (×10 ⁻²)	0.35±0.12	0.32±0.09	0.31±0.09	0.2

Data are presented as mean±SD or n (%), unless otherwise stated. BMI: body mass index; COVID-19: coronavirus disease 2019; SGRQ: St George's Respiratory Questionnaire; FEV₁: forced expiratory volume in 1 s; FVC: forced vital capacity; RV: residual volume; TLC: total lung capacity; D_{LCO}: diffusing capacity of the lung for carbon monoxide; VDP: ventilation defect percent; Mem/Gas: membrane-to-gas ratio (membrane uptake); RBC/Mem: red blood cell-to-membrane ratio; RBC/Gas: red blood cell-to-gas ratio (red blood cell transfer). [#]: PFT measurements included where available (COVID-negative: n=27 for FEV₁ and FVC, n=15 for RV, n=20 for TLC, n=21 for D_{LCO}; recovered: n=27 for all PFTs; long COVID: n=66 for FEV₁ and FVC, n=57 for RV, n=61 for TLC, n=62 for D_{LCO}); [¶]: using one-way ANOVA for parametric variables, Kruskal-Wallis tests for non-parametric variables or Fisher's exact test for categorical variables (bold p-values indicate p<0.05); [†]: SGRQ administered at Site 1 only (n=11 COVID-negative, n=26 recovered, n=36 long COVID); [§]: significantly different from COVID-negative (p<0.05); ^f: significantly different from recovered (p<0.05).

lowest scores in Cluster 1 and highest scores in Cluster 4 (post-hoc p=0.02). The proportion of participants hospitalised during the acute infection phase was significantly different across clusters (p=0.03), with the greatest proportion (63%) and the longest hospital stays (mean 28 days) in Cluster 4. Oxygen use (p=0.005), intensive care unit admission (p=0.001) and use of ventilation (p<0.001) during hospitalisation were significantly different across the clusters, again with the greatest proportions in Cluster 4 (80–100%). Dexamethasone and other steroids (60–100%) and remdesivir (antiviral, 14–67%) were the most common in-patient medical therapies across all clusters. Only the use of steroids was significantly different but borderline (p=0.045), with 100% of Cluster 1 and Cluster 3 patients prescribed steroids, followed by 71% of Cluster 2 and 60% of Cluster 4. Full details for acute hospitalisation interventions are provided in supplementary table E5. All ¹²⁹Xe MRI and most PFT measurements were significantly different across the clusters (p<0.05).

Up to 27% of all long COVID participants had at least one of the comorbidities: hypertension, diabetes, gastro-oesophageal reflux disease, obstructive sleep apnoea, asthma or COPD. There were no significant differences in the prevalence of specific comorbidities across clusters, although the median number of comorbidities per participant was significantly different (p=0.04) (supplementary table E6), with Cluster 3 and Cluster 4 trending to the most comorbidities (p=0.055 and p=0.054, respectively, *versus* Cluster 1). For those participants with asthma and COPD, prescribed respiratory medications are listed in supplementary table E7; most participants with asthma and COPD had mild disease based on international Global Initiative for Asthma (GINA) and Global Initiative for Chronic Obstructive Lung Disease (GOLD) guidelines, respectively, except two participants with asthma who had been prescribed dupilumab (Cluster 3) or prednisone (Cluster 4). All had well-controlled disease prior to the initial SARS-CoV-2 infection. There were no differences in respiratory medications across the clusters.

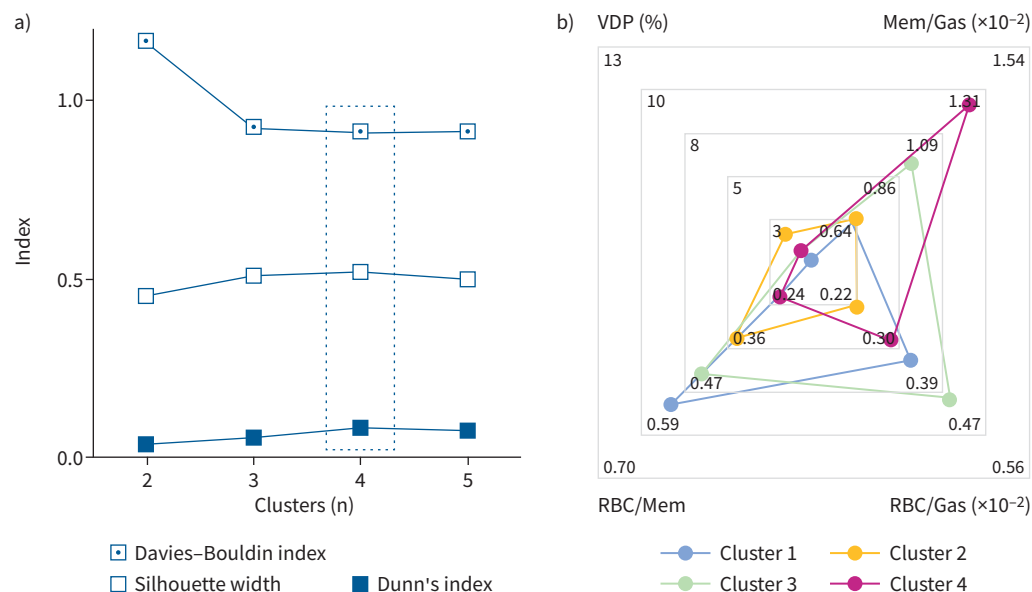


FIGURE 2 Internal cluster validation and primary ^{129}Xe magnetic resonance imaging (MRI) signatures for final clusters. **a)** Internal cluster validation using Davies-Bouldin index (minimised; 1.1644, 0.9236, **0.9132**, 0.9167), Dunn's index (maximised; 0.0356, 0.0535, **0.0832**, 0.0786) and silhouette width (maximised; 0.4521, 0.5122, **0.5223**, 0.4984) for two to five clusters. Four was the optimal number of clusters across all three indices (bold data values and dashed box). **b)** Radar plot showing the primary ^{129}Xe MRI signatures associated with each cluster. Scales show minimum and maximum for each MRI metric on one of the four radial axes and points represent mean cluster values. VDP: ventilation defect percent; Mem/Gas: membrane-to-gas ratio (membrane uptake); RBC/Mem: red blood cell-to-membrane ratio; RBC/Gas: red blood cell-to-gas ratio (red blood cell transfer).

Dyspnoea (85%) and fatigue (77%) were the most commonly reported symptoms among all long COVID participants and were common in all clusters (63–100%). The occurrence of ongoing symptoms was not significantly different across clusters.

A subset of 56 long COVID participants underwent chest CT for post-COVID assessment (range 180 days before to 99 days after MRI). Presence of GGOs, reticulation and consolidation was significantly different across the clusters ($p < 0.05$), with the most CT abnormalities being present in Cluster 4. Of note, all eight participants in Cluster 4 had evidence of GGOs. Representative ^{129}Xe MRI and CT images from each cluster as well as COVID-negative and recovered participants are shown in supplementary figure E2. CT was acquired with varied protocols across sites, thus further quantitative analysis could not be performed.

Figures 3 and 4 show cluster-wise comparisons with COVID-negative and recovered groups for MRI and clinical measurements, respectively, and full cluster-wise comparisons are provided in supplementary tables E8–E19. Of note, all clusters had a unique MRI feature compared with COVID-negative and fully recovered participants. SGRQ was different in all long COVID clusters, and trending greatest in Cluster 4. FEV₁, FVC, D_{LCO} , RV and TLC for most participants were above the lower limit of normal and were significantly different in Cluster 4 only. As a proof-of-concept to explain Cluster 1 pathophysiology, we tested RV/TLC for Cluster 1 only, which was significantly greater than COVID-negative participants ($p = 0.04$, independent samples t-test).

Altogether, the MRI and clinical features of each cluster are summarised in figure 5 with representative ^{129}Xe images. Cluster 1 exhibited “normal” ^{129}Xe MRI metrics but mildly increased RV/TLC relative to COVID-negative participants, and was the youngest group with no inspiratory CT parenchymal abnormalities and normal spirometry. Cluster 2 was characterised by low RBC/Mem only, and was the oldest group with mildly reduced D_{LCO} , no inspiratory CT parenchymal abnormalities, and normal spirometry and lung volumes. Cluster 3 was characterised by mildly elevated membrane uptake and preserved RBC/Mem, with minimal CT abnormalities and normal PFTs. Finally, Cluster 4 was characterised by markedly elevated membrane uptake and corresponding low RBC/Mem, with high body mass index, CT abnormalities, and reduced flow rates on spirometry, D_{LCO} and lung volumes.

TABLE 2 Long COVID magnetic resonance imaging (MRI) cluster summary[#]

	Cluster 1 (n=24)	Cluster 2 (n=22)	Cluster 3 (n=19)	Cluster 4 (n=8)	p-value [¶]
Age (years)	43±13	55±10	49±11	52±13	0.004
Female	12 (50)	15 (68)	12 (63)	5 (63)	0.6
Caucasian	20 (83)	19 (86)	17 (89)	6 (75)	0.2
BMI (kg·m ⁻²)	26±4	28±5	31±8	33±7	0.02
Hospitalised for COVID-19 during acute infection	3 (13)	7 (32)	3 (16)	5 (63)	0.03
Time between COVID-19 diagnosis and MRI (days)	429±222	446±246	381±191	358±276	0.7
SGRQ Total [†]	31±23	36±14	37±16	60±13	0.2
SGRQ Symptom [†]	42±24	39±17	39±26	59±14	0.6
SGRQ Activity [†]	37±29	57±16	57±17	84±4	0.02
SGRQ Impact [†]	24±24	22±17	23±16	46±21	0.4
FEV ₁ (% pred)	100±15	101±19	104±18	82±22	0.057
FVC (% pred)	107±15	103±20	105±18	79±23	0.005
FEV ₁ /FVC (%)	76±6	79±6	81±6	85±4	0.005
RV (% pred)	118±24	104±34	103±24	71±29	0.006
TLC (% pred)	100±14	95±19	95±15	70±20	0.002
RV/TLC (% pred)	118±17	111±30	110±21	103±24	0.4
D _{LCO} (% pred)	109±18	93±20	108±18	61±29	<0.001
VDP (%)	0±0	2±3	1±1	1±1	0.004
Mem/Gas (×10 ⁻²)	0.62±0.09	0.64±0.14	0.92±0.14	1.23±0.19	<0.001
RBC/Mem	0.51±0.07	0.33±0.07	0.42±0.08	0.22±0.06	<0.001
RBC/Gas (×10 ⁻²)	0.33±0.06	0.22±0.05	0.40±0.07	0.29±0.09	<0.001
Comorbidities					
Hypertension	2 (8)	7 (32)	6 (32)	4 (50)	0.052
Diabetes	0 (0)	1 (5)	4 (21)	2 (25)	0.06
GORD	3 (13)	9 (41)	4 (21)	1 (13)	0.1
OSA	4 (17)	4 (18)	6 (32)	2 (25)	0.7
Asthma	5 (21)	8 (36)	6 (32)	1 (13)	0.5
COPD	0 (0)	1 (5)	1 (5)	0 (0)	0.6
Persistent symptoms					
Dyspnoea	19 (79)	21 (95)	14 (74)	8 (100)	0.5
Chest tightness	6 (25)	9 (41)	3 (16)	1 (13)	0.2
Cough	6 (25)	6 (27)	5 (26)	3 (38)	0.6
Fatigue	15 (63)	19 (86)	17 (89)	5 (63)	0.2
Nausea	2 (8)	3 (14)	3 (16)	0 (0)	0.8
Loss of taste/smell	9 (38)	5 (23)	2 (11)	2 (25)	0.4
CT patterns[§]	(n=19)	(n=14)	(n=15)	(n=8)	
GGOs	0 (0)	1 (7)	1 (7)	8 (100)	<0.001
Reticulation	0 (0)	2 (14)	2 (13)	3 (38)	0.046
Honeycombing	0 (0)	0 (0)	0 (0)	1 (13)	0.1
Consolidation	0 (0)	0 (0)	0 (0)	2 (25)	0.02
Emphysema	1 (5)	1 (7)	0 (0)	0 (0)	0.8

Data are presented as mean±SD or n (%), unless otherwise stated. BMI: body mass index; COVID-19: coronavirus disease 2019; SGRQ: St George's Respiratory Questionnaire; FEV₁: forced expiratory volume in 1 s; FVC: forced vital capacity; RV: residual volume; TLC: total lung capacity; D_{LCO}: diffusing capacity of the lung for carbon monoxide; VDP: ventilation defect percent; Mem/Gas: membrane-to-gas ratio (membrane uptake); RBC/Mem: red blood cell-to-membrane ratio; RBC/Gas: red blood cell-to-gas ratio (red blood cell transfer); GORD: gastro-oesophageal reflux disease; OSA: obstructive sleep apnoea; CT: computed tomography; GGO: ground-glass opacity. [#]: pulmonary function test measurements included where available (all long COVID: n=66 for FEV₁ and FVC, n=57 for RV, n=61 for TLC, n=62 for D_{LCO}; Cluster 1: n=23 for FEV₁ and FVC, n=21 for RV, n=22 for TLC, n=22 for D_{LCO}; Cluster 2: n=18 for FEV₁ and FVC, n=15 for RV, n=17 for TLC, n=17 for D_{LCO}; Cluster 3: n=18 for FEV₁ and FVC, n=15 for RV, n=16 for TLC, n=16 for D_{LCO}; Cluster 4: n=7 for FEV₁ and FVC, n=6 for RV, TLC, n=7 for D_{LCO}); [¶]: p-values shown for long COVID cluster comparisons only: using one-way ANOVA for parametric variables, Kruskal-Wallis tests for non-parametric variables or Fisher's exact test for categorical variables (bold p-values indicate p<0.05); [†]: SGRQ administered at Site 1 only (n=15 Cluster 1, n=6 Cluster 2, n=8 Cluster 3, n=3 Cluster 4); [§]: CT patterns identified as present or absent by qualitative radiologist review (percentages shown as fraction of subset of patients with CT in each cluster).

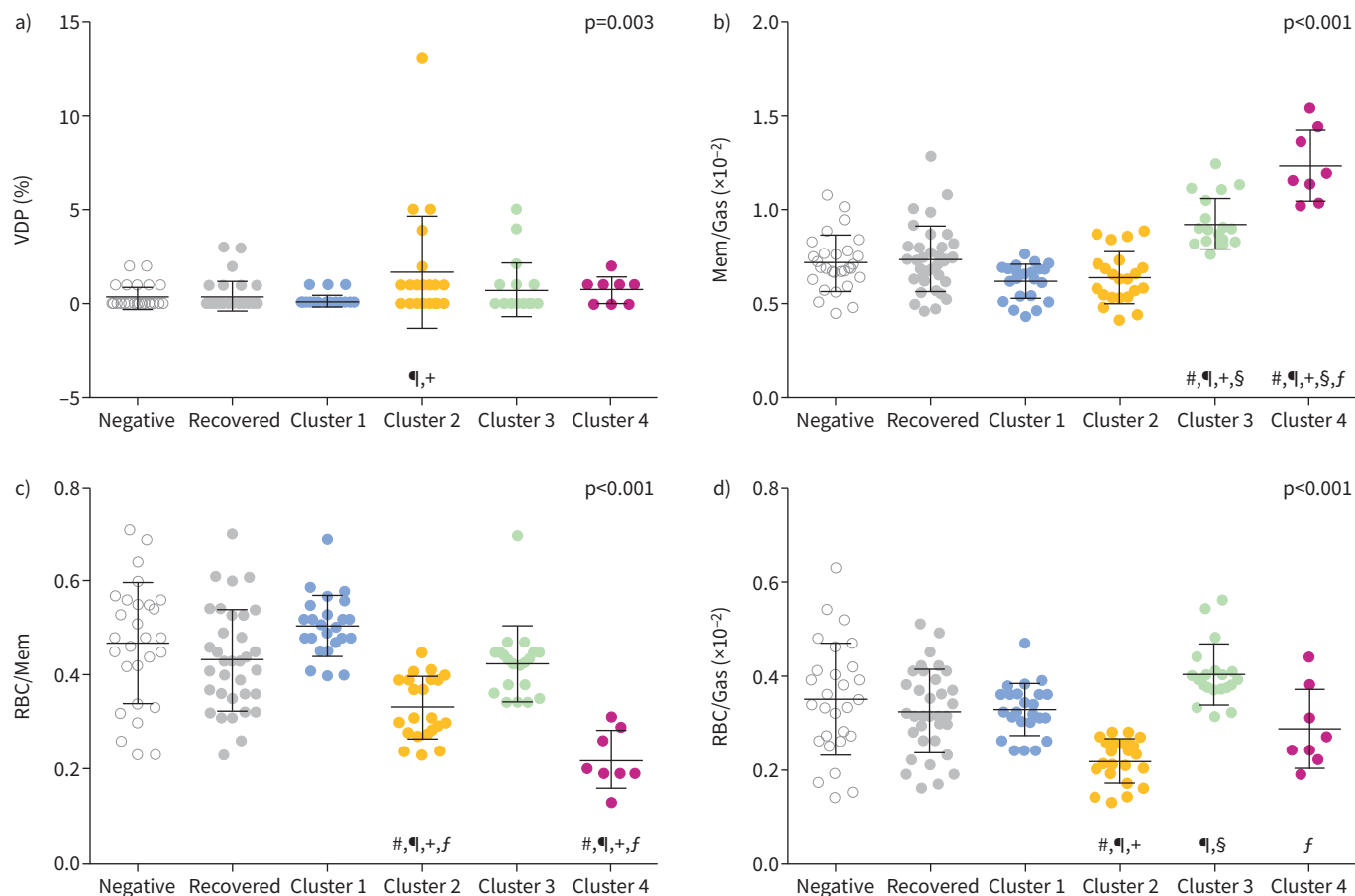


FIGURE 3 Magnetic resonance imaging (MRI) measurement comparison by cluster. Comparison of four MRI measurements used to generate long COVID clusters against COVID-negative and fully recovered participants for a) ventilation defect percent (VDP), b) membrane-to-gas (Mem/Gas) ratio (membrane uptake), c) red blood cell-to-membrane (RBC/Mem) ratio and d) red blood cell-to-gas (RBC/Gas) ratio (red blood cell transfer). Symbols signify significant differences ($p < 0.05$): #: versus COVID-negative; †: versus recovered; ‡: versus Cluster 1; §: versus Cluster 2; ¶: versus Cluster 3.

Discussion

In this multicentre study, we identified four long COVID clusters with unique ^{129}Xe MRI signatures and corresponding distinct demographic and clinical features. The key strength of this work is the large multicentre population with harmonised ^{129}Xe imaging acquisition and analysis methods, thereby enabling cluster analysis to discover data-driven phenotypic subtypes of long COVID. Previously published ^{129}Xe MRI studies have revealed low RBC/Mem in people with post-acute or long COVID [13–17, 35], consistent with the Cluster 2 phenotype in our work [15, 17]. We further identified three other functional pulmonary long COVID groups. Cluster 1 exhibited normal ^{129}Xe MRI with mildly increased RV/TLC and elevated SGRQ. Cluster 3 and Cluster 4 were uniquely driven by elevated ^{129}Xe membrane uptake that has not been previously noted in long COVID participants [13–17, 35]. Prior reports have also shown abnormal VDP that was related to worse quality of life and exercise limitation in long COVID [11, 12]; while VDP was greatest in Cluster 2, the burden of ventilation abnormalities was low in all clusters. Thus, gas exchange abnormalities, and not airway or ventilation, were the greatest pathophysiological drivers of long COVID in these participants. We additionally showed that the characteristic ^{129}Xe gas exchange metrics in Clusters 2–4 were different from both COVID-negative controls and fully recovered participants.

The heterogeneity of long COVID has made it challenging to advance clinical understanding and develop novel therapies. Here, we used an emerging technology, ^{129}Xe MRI, to dissect the heterogeneity of long COVID and found that there are several clusters of physiological processes that underpin the condition. There is a cluster of patients (Cluster 1, ~30% of participants) who have mildly elevated RV/TLC ratio indicating air trapping despite “normal” MRI and inspiratory CT. This group of long COVID patients may be similar to those from prior work that showed air trapping using expiratory CT [10]. For Cluster 1, we

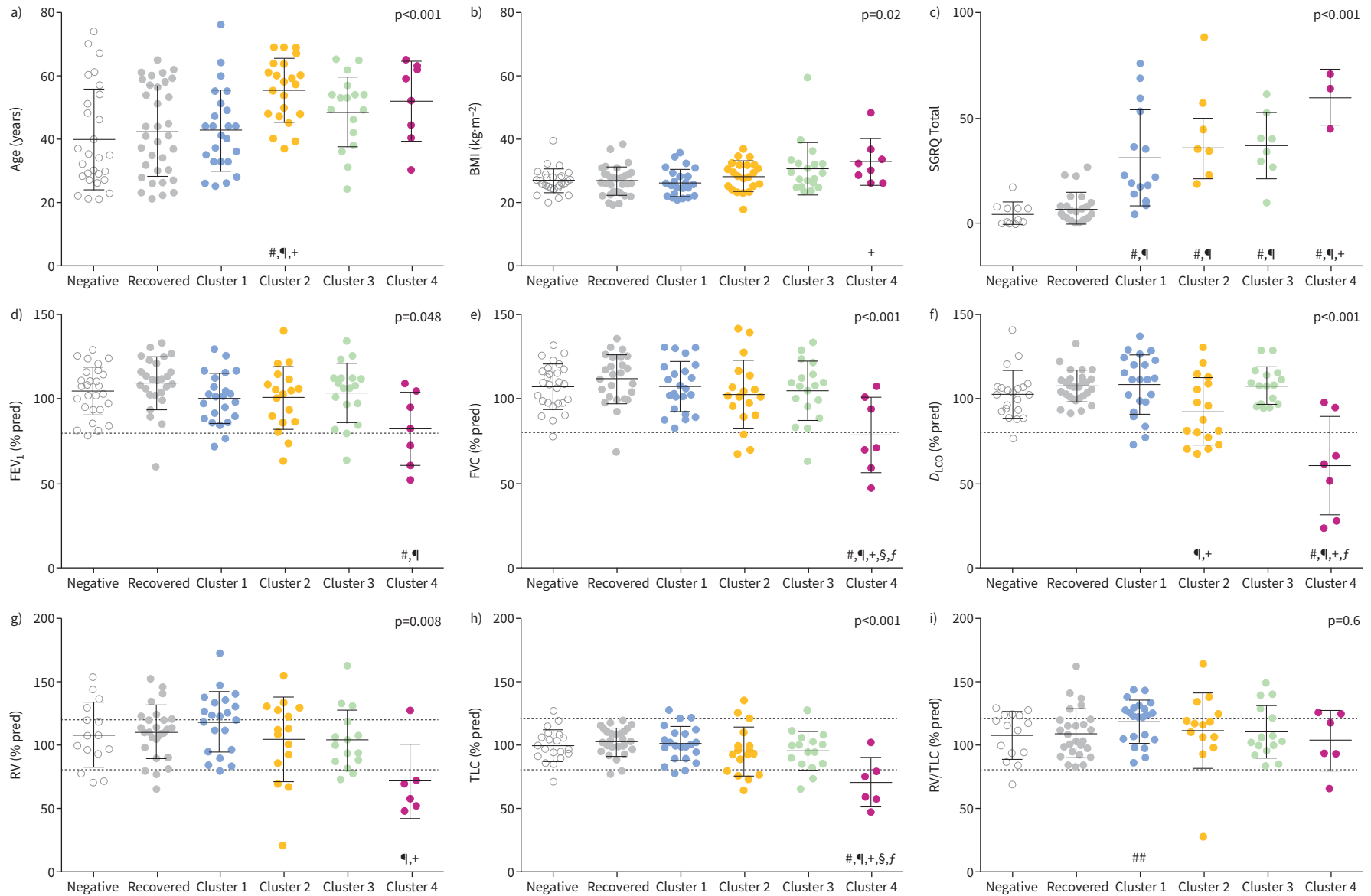


FIGURE 4 Demographic and pulmonary function test (PFT) measurement comparison by cluster. Comparison of clinical characteristics across COVID-negative, recovered and long COVID clusters for a) participant age, b) body mass index (BMI), c) St George’s Respiratory Questionnaire (SGRQ) Total score, d) forced expiratory volume in 1 s (FEV₁), e) forced vital capacity (FVC), f) diffusing capacity of the lung for carbon monoxide (D_{LCO}), g) residual volume (RV), h) total lung capacity (TLC) and i) RV/TLC. Dotted grey lines show lower and/or upper limits of normal for PFTs. p-values in graphs are from ANOVA comparing all six groups. Symbols signify significant group-wise differences after Bonferroni correction (p<0.05): #: versus COVID-negative; ¶: versus recovered; †: versus Cluster 1; §: versus Cluster 2; f: versus Cluster 3. ##: as a proof-of-concept using an independent samples t-test, Cluster 1 RV/TLC was significantly greater than COVID-negative (p=0.04).

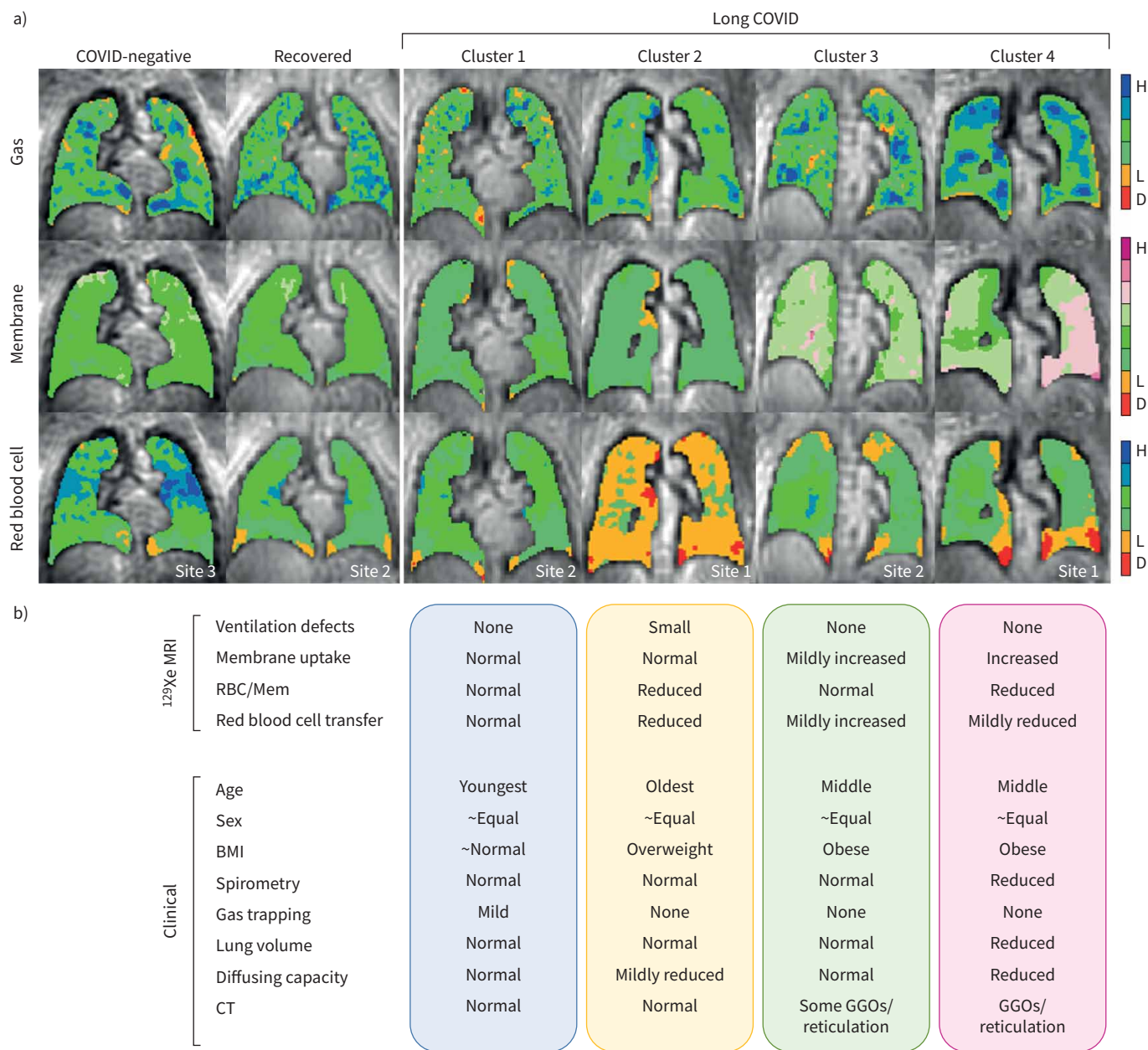


FIGURE 5 Long COVID cluster summary. a) ¹²⁹Xe magnetic resonance gas, membrane and red blood cell images for representative participants in the COVID-negative group, the recovered group and resulting long COVID clusters. The site location for each participant is embedded in the images. b) Qualitative cluster comparison for imaging measurements used to generate clusters and clinical characteristics. D: defect (no signal); L: low-intensity signal; H: high-intensity signal; RBC/Mem: red blood cell-to-membrane ratio; BMI: body mass index; CT: computed tomography; GGO: ground-glass opacity.

posit that bronchodilators could be effective in relieving gas trapping [12], although future studies are needed to validate this notion.

We were also able to separate participants with low RBC/Mem alone (Cluster 2, ~30% of participants) from those with low RBC/Mem concomitant with elevated membrane uptake (Cluster 4, ~10% of participants) and those with elevated membrane uptake but preserved RBC/Mem (Cluster 3, ~30% of participants). Low RBC/Mem in Cluster 2 in the absence of airway or parenchymal abnormalities adds to the growing evidence [13–17, 35] of post-COVID microvascular abnormalities such as pulmonary capillary inflammation, vasoconstrictive remodelling or thrombosis that inhibit transfer of gas [18, 36]. Cluster 3

was only differentiated by mildly elevated Mem/Gas (with preserved RBC/Mem), which may represent (residual) interstitial inflammation or oedema. Cluster 2 and Cluster 3 signatures demonstrate the high sensitivity of ^{129}Xe MRI in revealing abnormalities in specific components of pulmonary gas exchange pathophysiology. In contrast, D_{LCO} provides a whole-lung average of the alveolar epithelial–capillary structure, which may explain why participants in Cluster 2 and Cluster 3 had D_{LCO} values all within normal limits. These data also raise the possibility of evaluating specific anti-inflammatory therapies targeted at the alveolar–capillary units as well as non-pharmacological interventions such as pulmonary rehabilitation and exercise for patients in these clusters to enhance gas exchange and reduce symptoms.

Cluster 4 had considerably elevated ^{129}Xe membrane uptake with concomitant low RBC/Mem and gas transfer, restrictive pattern on PFTs, GGOs on CT, and the highest SGRQ, indicating worse respiratory health status. Although small, Cluster 4 was largely comprised of participants with the greatest severity of acute COVID-19 (based on hospitalisation and in-patient interventions) and who were left with persistent post-COVID interstitial lung abnormalities [37]. It should be noted, however, that around a third of all participants in Cluster 4 did not require hospitalisation for acute COVID-19. Thus, while severe COVID-19 pneumonia is a risk factor for Cluster 4, patients who had milder COVID-19 infection can remain highly symptomatic 1–2 years following their initial infection. ^{129}Xe gas exchange MRI is known to be sensitive in detecting abnormalities in advanced interstitial lung disease [38–40]; however, the observed increase in ^{129}Xe membrane uptake and CT patterns in Cluster 4 were not as extensive, suggesting early or mild stages of any post-COVID interstitial abnormalities. Cluster 3 and Cluster 4 long COVID participants could be targeted for monitoring to determine whether ^{129}Xe membrane uptake in this context is a treatable trait and whether these changes are permanent or transient. Long-term longitudinal studies will also be of value in determining whether there is a natural progression of clusters from Cluster 1 to Cluster 4 (or from Cluster 4 to Cluster 1) over time or whether each of these clusters are distinct phenotypes with different molecular drivers.

The impact of persistent symptoms was corroborated with elevated SGRQ across all clusters compared with COVID-negative and fully recovered post-COVID participants; however, there were no significant differences in self-reported symptoms across the clusters. Our study was likely underpowered to draw such conclusions because of the symptoms which were recorded and could be pooled from all sites. For example, “brain fog” has more recently been recognised as a common long COVID symptom [9], but neurocognitive symptoms were not recorded. However, respiratory symptoms relevant to ^{129}Xe MRI including dyspnoea, chest tightness and cough were highly prevalent in these participants. We note that although asthma was the most commonly reported respiratory comorbidity, the overall burden of pre-existing respiratory disease was low and non-severe. Ongoing respiratory symptoms in all patients were adjudicated as new or worse post-COVID and thus mostly likely to be COVID-19 related. Furthermore, Cluster 4 had the greatest SGRQ Total score and significantly greater SGRQ Activity score (*versus* Cluster 1), indicating worse respiratory-related quality of life and activity limitation related to dyspnoea, and consistent with the most severe ^{129}Xe MRI changes in this group.

Limitations

Limitations of our study include the site-specific study designs and retrospective aggregation of multicentre data, which limited comparisons of some clinical information. Importantly, MRI data quality and measurements were validated across sites to ensure data compatibility for clustering. This study was also cross-sectional where MRI was not performed at a pre-specified interval following SARS-CoV-2 infection at any site, and PFTs and CT were not always performed contemporaneously with MRI. As a result, we cannot be certain on how measurements in each of the clusters or recovered group evolved over time, nor whether MRI differences might be related to different pulmonary effects of SARS-CoV-2 between participants. We note, however, that prior longitudinal studies showed negligible change in RBC/Mem between ~3 and 15 months post-infection [15, 17]. CT was not performed with a consistent protocol at all sites, so quantification nor regional comparisons of CT patterns could not be performed. It is unknown how post-COVID MRI findings compare with acute lung injury caused by other infectious agents such as influenza. Peripheral blood was also not collected to help further characterise MRI measurements and phenotypes. However, a subset of participants from Site 1 underwent bronchoscopy and sample of small airways; these results will be reported separately. Furthermore, like most long COVID research to date, pre-COVID-19 measurements were not available for comparison in these participants.

We were also unable to confirm COVID-19 variants to compare whether different variants contribute to differences across clusters. We posit based on the self-reported COVID-19 testing dates that most infections were pre-omicron. Acute SARS-CoV-2 infection dates spanned timelines before vaccinations were available in the local regions and after up to two vaccine doses, therefore we did not evaluate the

impact of vaccination on MRI abnormalities or differences across the clusters. Finally, COVID-19 antibody testing was not performed to verify self-reported SARS-CoV-2 infection status.

Conclusions

In conclusion, we demonstrate four unique long COVID phenotypes defined by ^{129}Xe MRI metrics, with distinct functional MRI and corresponding clinical characteristics. Such differences were otherwise not evident in the total long COVID group compared with COVID-negative and fully recovered post-COVID participants, especially using PFTs and CT. These four clusters reveal distinct (patho-)physiological changes that can be potential targets for therapy. Although a relatively new technology, ^{129}Xe MRI is now approved for clinical use in the UK and USA [31], providing new clinical opportunities for improved characterisation of respiratory diseases [38] and targeting of therapeutics for patients with long COVID. Future work can build from this foundation towards personalised medicine to evaluate the biological underpinnings of ^{129}Xe MRI signatures of long COVID clusters, and to determine their disease trajectories and responses to therapy.

Ethics statement: Participants provided written informed consent to ethics board-approved studies across three centres.

Conflicts of interest: R.L. Eddy reports grants from Michael Smith Health Research BC, Canadian Respiratory Research Network, and Natural Sciences and Engineering Research Council Canada, consulting fees from VIDA Diagnostics Inc., payment or honoraria for lectures from Thorasys Thoracic Medical Systems Inc., support for attending meetings and/or travel from the Canadian Institutes of Health Research – Institute of Circulatory and Respiratory Health, and a leadership or fiduciary role for the Xenon MRI Clinical Trials Consortium (Steering Committee Member). D. Mummy reports consultancy fees from Polarean Imaging Plc. F.V. Gerayeli reports grants from MITACS Accelerate. J.A. Leipsic reports grants from GE Healthcare, consultancy fees and support for attending meetings and/or travel from Heartflow, and owns stock/stock options in Heartflow. J.M. Leung reports grants from the Canadian Institutes of Health Research and BC Lung Foundation, payment or honoraria for lectures, presentations, manuscript writing or educational events from the BC Lung Foundation, participation on a data safety monitoring board or advisory board for Enhance Quality Safety, and Patient Experience in Chronic Obstructive Pulmonary Disorder (EQUIP COPD), and leadership or fiduciary roles for the Canadian Respiratory Research Network and CanCOLD Study. B. Driehuys reports grants from Translating Duke Health (Duke Internal Award), royalties or licenses from Polarean Imaging, a leadership or fiduciary role with Polarean Imaging, and owns stock/stock options in Polarean Imaging. L.G. Que reports grants from Translating Duke Health (Duke Internal Award) and a leadership or fiduciary role as a member of the Xe MRI Consortium. M. Castro reports grants from the NIH, ALA, PCORI, AstraZeneca, Gala Therapeutics, Genentech, GSK, Novartis, Pulmatrix, Sanofi-Aventis, Shionogi and Theravance, consulting fees from Genentech, Teva, Sanofi-Aventis, Merck, Novartis, Arrowhead Pharmaceuticals, Allakos, Amgen, OM Pharma, Pfizer, Pioneering Medicines and GSK, payment or honoraria for lectures, presentations, manuscript writing or educational events from Amgen, AstraZeneca, Genentech, Regeneron, Sanofi-Aventis and Teva, and owns stock/stock options in Aer Therapeutics. D.D. Sin reports payment or honoraria for lectures, presentations, manuscript writing or educational events from GSK, AstraZeneca and Boehringer Ingelheim, and participation on a data safety monitoring board or advisory board for the NHLBI. P.J. Niedbalski reports grants from the Scleroderma Foundation (New Investigator Grant) and American Heart Association (CDA 930177), and consultancy fees, payment or honoraria for lectures, and support for attending meetings and/or travel from Polarean Imaging Plc. The remaining authors have no potential conflicts of interest to disclose.

Support statement: This work was supported by the Canadian Institutes of Health Research (CIHR) and St Paul's Foundation (Site 1, University of British Columbia); and Translating Duke Health – Keeping the Heart Young Pilot Award and NHLBI R01HL126771 (Site 3, Duke University). Funding information for this article has been deposited with the Crossref Funder Registry.

References

- 1 National Institute for Health and Care Excellence. COVID-19 rapid guideline: managing the long-term effects of COVID-19. 2020. www.nice.org.uk/guidance/ng188 Date last accessed: 2 February 2024.
- 2 US Centers for Disease Control and Prevention. Long COVID or post-COVID conditions. 2023. www.cdc.gov/coronavirus/2019-ncov/long-term-effects/index.html Date last accessed: 4 September 2023.
- 3 World Health Organisation. A clinical case definition of post COVID-19 condition by a Delphi consensus. 2021. www.who.int/publications/i/item/WHO-2019-nCoV-Post_COVID-19_condition-Clinical_case_definition-2021.1 Date last accessed: 2 February 2024.

- 4 Global Burden of Disease Long COVID Collaborators. Estimated global proportions of individuals with persistent fatigue, cognitive, and respiratory symptom clusters following symptomatic COVID-19 in 2020 and 2021. *JAMA* 2022; 328: 1604–1615.
- 5 Chen C, Hauptert SR, Zimmermann L, et al. Global prevalence of post-coronavirus disease 2019 (COVID-19) condition or long COVID: a meta-analysis and systematic review. *J Infect Dis* 2022; 226: 1593–1607.
- 6 Davis HE, McCorkell L, Vogel JM, et al. Long COVID: major findings, mechanisms and recommendations. *Nat Rev Microbiol* 2023; 21: 133–146.
- 7 Ford ND, Slaughter D, Edwards D, et al. Long COVID and significant activity limitation among adults, by age – United States, June 1–13, 2022, to June 7–19, 2023. *MMWR Morb Mortal Wkly Rep* 2023; 72: 866–870.
- 8 Bowe B, Xie Y, Al-Aly Z. Postacute sequelae of COVID-19 at 2 years. *Nat Med* 2023; 29: 2347–2357.
- 9 Perlis RH, Santillana M, Ognyanova K, et al. Prevalence and correlates of long COVID symptoms among US adults. *JAMA Netw Open* 2022; 5: e2238804.
- 10 Cho JL, Villacreses R, Nagpal P, et al. Quantitative chest CT assessment of small airways disease in post-acute SARS-CoV-2 infection. *Radiology* 2022; 304: 185–192.
- 11 Kooner HK, McIntosh MJ, Matheson AM, et al. ^{129}Xe MRI ventilation defects in ever-hospitalised and never-hospitalised people with post-acute COVID-19 syndrome. *BMJ Open Respir Res* 2022; 9: e001235.
- 12 Kooner HK, McIntosh MJ, Matheson AM, et al. Post-acute COVID-19 syndrome: ^{129}Xe MRI ventilation defects and respiratory outcomes one year later. *Radiology* 2023; 307: e222557.
- 13 Grist JT, Chen M, Collier GJ, et al. Hyperpolarized ^{129}Xe MRI abnormalities in dyspneic patients 3 months after COVID-19 pneumonia: preliminary results. *Radiology* 2021; 301: E353–E360.
- 14 Grist JT, Collier GJ, Walters H, et al. Lung abnormalities depicted with hyperpolarized xenon MRI in patients with long COVID. *Radiology* 2022; 305: 709–717.
- 15 Saunders LC, Collier GJ, Chan HF, et al. Longitudinal lung function assessment of patients hospitalised with COVID-19 using ^1H and ^{129}Xe lung MRI. *Chest* 2023; 164: 700–716.
- 16 Matheson AM, McIntosh MJ, Kooner HK, et al. Persistent ^{129}Xe MRI pulmonary and CT vascular abnormalities in symptomatic individuals with post-acute COVID-19 syndrome. *Radiology* 2022; 305: 466–476.
- 17 Matheson AM, McIntosh MJ, Kooner HK, et al. Longitudinal follow-up of postacute COVID-19 syndrome: DL_{CO}, quality-of-life and MRI pulmonary gas-exchange abnormalities. *Thorax* 2023; 78: 418–421.
- 18 Ackermann M, Verleden SE, Kuehnel M, et al. Pulmonary vascular endothelialitis, thrombosis, and angiogenesis in Covid-19. *N Engl J Med* 2020; 383: 120–128.
- 19 Subramanian A, Nirantharakumar K, Hughes S, et al. Symptoms and risk factors for long COVID in non-hospitalized adults. *Nat Med* 2022; 28: 1706–1714.
- 20 Zhang H, Zang C, Xu Z, et al. Data-driven identification of post-acute SARS-CoV-2 infection subphenotypes. *Nat Med* 2023; 29: 226–235.
- 21 Danesh V, Arroliga AC, Bourgeois JA, et al. Symptom clusters seen in adult COVID-19 recovery clinic care seekers. *J Gen Intern Med* 2023; 38: 442–449.
- 22 Choi S, Hoffman EA, Wenzel SE, et al. Quantitative computed tomographic imaging-based clustering differentiates asthmatic subgroups with distinctive clinical phenotypes. *J Allergy Clin Immunol* 2017; 140: 690–700.
- 23 Eddy RL, McIntosh MJ, Matheson AM, et al. Pulmonary MRI and cluster analysis help identify novel asthma phenotypes. *J Magn Reson Imaging* 2022; 56: 1475–1486.
- 24 Billatos E, Ash SY, Duan F, et al. Distinguishing smoking-related lung disease phenotypes via imaging and molecular features. *Chest* 2021; 159: 549–563.
- 25 Eddy RL, Mummy D, Dai H, et al. ^{129}Xe magnetic resonance imaging-based phenotypes of long COVID: a multi-center evaluation. *Am J Respir Crit Care Med* 2023; 207: A6786.
- 26 Jones PW, Quirk FH, Baveystock CM. The St George's Respiratory Questionnaire. *Respir Med* 1991; 85: Suppl. B, 25–31.
- 27 Miller MR, Hankinson J, Brusasco V, et al. Standardisation of spirometry. *Eur Respir J* 2005; 26: 319–338.
- 28 Wanger J, Clausen JL, Coates A, et al. Standardisation of the measurement of lung volumes. *Eur Respir J* 2005; 26: 511–522.
- 29 Graham BL, Brusasco V, Burgos F, et al. 2017 ERS/ATS standards for single-breath carbon monoxide uptake in the lung. *Eur Respir J* 2017; 49: 1600016.
- 30 Bowerman C, Bhakta NR, Brazzale D, et al. A race-neutral approach to the interpretation of lung function measurements. *Am J Respir Crit Care Med* 2023; 207: 768–774.
- 31 Niedbalski PJ, Hall CS, Castro M, et al. Protocols for multi-site trials using hyperpolarized ^{129}Xe MRI for imaging of ventilation, alveolar-airspace size, and gas exchange: a position paper from the ^{129}Xe MRI Clinical Trials Consortium. *Magn Reson Med* 2021; 86: 2966–2986.
- 32 Niedbalski PJ, Willmering MM, Thomen RP, et al. A single-breath-hold protocol for hyperpolarized ^{129}Xe ventilation and gas exchange imaging. *NMR Biomed* 2023; 36: e4923.
- 33 Niedbalski PJ, Lu J, Hall CS, et al. Utilizing flip angle/TR equivalence to reduce breath hold duration in hyperpolarized ^{129}Xe 1-point Dixon gas exchange imaging. *Magn Reson Med* 2022; 87: 1490–1499.

- 34 Wang Z, Robertson SH, Wang J, *et al.* Quantitative analysis of hyperpolarized ^{129}Xe gas transfer MRI. *Med Phys* 2017; 44: 2415–2428.
- 35 Li H, Zhao X, Wang Y, *et al.* Damaged lung gas exchange function of discharged COVID-19 patients detected by hyperpolarized ^{129}Xe MRI. *Sci Adv* 2021; 7: eabc8180.
- 36 Varga Z, Flammer AJ, Steiger P, *et al.* Endothelial cell infection and endotheliitis in COVID-19. *Lancet* 2020; 395: 1417–1418.
- 37 Stewart I, Jacob J, George PM, *et al.* Residual lung abnormalities after COVID-19 hospitalization: interim analysis of the UKILD post-COVID-19 study. *Am J Respir Crit Care Med* 2023; 207: 693–703.
- 38 Wang Z, Bier EA, Swaminathan A, *et al.* Diverse cardiopulmonary diseases are associated with distinct xenon magnetic resonance imaging signatures. *Eur Respir J* 2019; 54: 1900831.
- 39 Collier GJ, Eaden JA, Hughes PJC, *et al.* Dissolved ^{129}Xe lung MRI with four-echo 3D radial spectroscopic imaging: quantification of regional gas transfer in idiopathic pulmonary fibrosis. *Magn Reson Med* 2021; 85: 2622–2633.
- 40 Mummy DG, Bier EA, Wang Z, *et al.* Hyperpolarized ^{129}Xe MRI and spectroscopy of gas-exchange abnormalities in nonspecific interstitial pneumonia. *Radiology* 2021; 301: 211–220.